On-Line Analysis/Synthesis-Based Channel Parameters Estimation and Wideband CDMA Receiver Design Verification

Karim Cheikhrouhou*, Sofiène Affes*, Ahmed Elderini*, Besma Smida*, Paul Mermelstein*,
Belhassen Sultana† and Venkatesh Sampath‡
*INRS-ÉMT, Université du Québec, Montreal, Canada - {cheikhro,affes,elderini,smida,mermel}@emt.inrs.ca
†Microcell Solutions, Inc., Montreal, Canada - Belhassen.sultana@fidomobile.ca
‡Flarion Technologies, Bedminster, USA - V.Sampath@flarion.com

***Abstract*— The spatio-temporal array-receiver (STAR) decomposes the wideband CDMA channel responses along various parameter dimensions (*e.g.*, time delays, multipath components, etc...) and extracts the associated time-varying parameters (*i.e.*, analysis) before reconstructing the channel (*i.e.*, synthesis) with increased accuracy. This work verifies the channel analysis/synthesis design of STAR by illustrating its capability to extract accurately the channel parameters (time delays and drifts, carrier frequency offsets, Doppler spread, etc...) from measured data and to adapt online to their observed time evolution in real-world propagation conditions.**

I. Introduction

Motivated by the need for increased bandwidth efficiencies, we have recently developed a new spatio-temporal array-receiver (STAR) [1] that achieves accurate and fast temporal synchronization, channel identification and efficient signal combining with significant gains in performance over RAKE-type receivers [1]. More recently, we upgraded STAR to integrate space-time multi-user detection based on interference subspace rejection (ISR) [2], carrier frequency offset (CFO) recovery (CFOR) [3]. All these significant enhancements exploit the powerful dynamic channel parameter extraction capabilities of STAR based on *a priori* known generic models for these parameters. Indeed, STAR applies an **"analysis/synthesis"** principle where it decomposes the channel over various channel parameter dimensions (*e.g.*, time delays, shaping pulse, Rayleigh fades, etc...), estimates those time-varying parameters (*i.e.*, analysis) then uses them to reconstruct the channel (*i.e.*, synthesis) with increased accuracy [1]. Verification of the software design of STAR using real-world channel measurements is an important step toward practical receiver implementation.

In this work, we verify the analysis/synthesis-based design of STAR by assessing its ability to extract online the channel parameters (time delays and drifts, multipath components and average multipath power profiles, CFOs, Doppler spread or speed) from 5 MHz radio-channels measured at 2 GHz [4].

In the recent context where **adaptive** receivers find very efficient use in wireless communications, it becomes essential not only to estimate the statistics of the wireless channel, but to have a very thorough understanding of the time realizations of its parameters and from there identify ways to reduce the imperfection of their generic time evolution models on which heavily depends the performance of adaptive 3G/3G+ receivers such as STAR.

II. Data Model and Overview of STAR

A. Data Model

For the sake of simplicity, we consider the uplink direction of a cellular CDMA system where each base-station is equipped with M receiving antennas. We further consider a selective fading multipath environment characterized by P propagation paths where the time delay spread $\Delta\tau$ is assumed small compared to T. The user's BPSK symbol sequence is first differentially encoded at rate $1/T$ where T is the symbol duration. The resulting sequence $b(t)$ is then spread with a long personal PN code $c(t)$ at a rate $1/T_c$ where T_c is the chip pulse duration. The spreading factor is given by $L = T/T_c$.

After sampling at the chip rate and framing over $2L-1$ chip samples at the symbol rate by the preprocessing unit, we obtain the $M \times (2L-1)$ matched-filtering observation matrix $\mathbf{Y}_n$. After despreading $\mathbf{Y}_n$ row-wise and framing the resulting post-correlation vector over L chip samples at the symbol rate, we obtain the $M \times L$-dimensional post-correlation observation matrix $\mathbf{Z}_n$ [1]:

$$\mathbf{Z}_n = s_n \underbrace{\mathbf{H}_n}_{\text{ST channel}} + \mathbf{N}_n = s_n \underbrace{\left(\mathbf{J}_n \mathbf{D}_n^T\right)}_{\text{ST analysis}} + \mathbf{N}_n \ , \quad (1)$$

where $s_n = b_n \psi_n$ denotes the signal component, $b_n = b(nT)$ is the transmitted DBPSK symbol and ψ_n^2 is the total received power affected by the Doppler spread and multipath fading, the path-loss and shadowing and power control (PC). $\mathbf{H}_n$ is the $M \times L$ spatio-temporal channel matrix. $\mathbf{N}_n$ is the $M \times L$ spatio-temporal noise matrix after despreading with variance σ_N^2. It includes the thermal noise received at the antenna elements as well as the self-, in-cell and out-cell interference. We hence define the input SNR after despreading as $SNR = \bar{\psi}^2/\sigma_N^2$ where $\bar{\psi}^2$ denotes the average received power.

The most important feature in the equation above, referred to as the post-correlation model (PCM) in [1], is the spatial-temporal (ST) **"analysis"** of the channel

0-7803-9152-7/05/$20.00 © 2005 IEEE

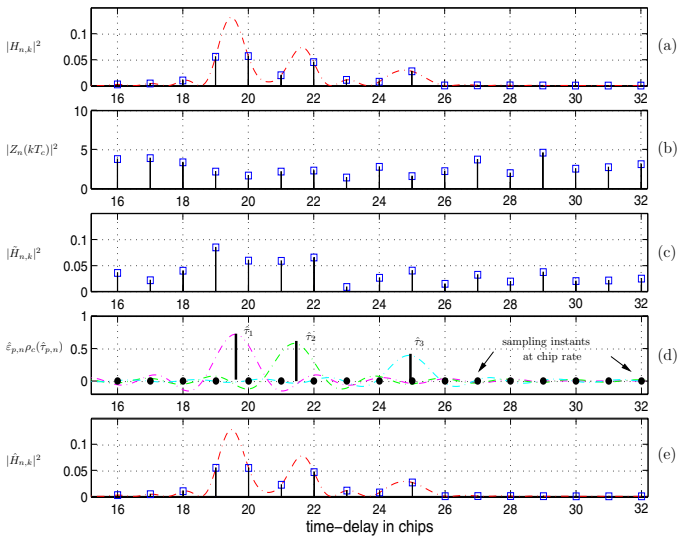

Fig. 1. Channel analysis/synthesis in STAR illustrated with $M = 1$ receive antenna: (a) power of chip-rate channel coefficients (power waveform is in dashed line), (b) power of chip-rate despread observation, (c) power of unconstrained estimate of chip-rate channel coefficients, (d) channel analysis by high-resolution extraction from $\tilde{\mathbf{H}}_n$ of time delays $\hat{\tau}_{p,n}$ and their number $\hat{P} = 3$, (e) power of constrained estimate of chip-rate channel coefficients after synthesis (resulting power waveform is in dashed line) by summation of $\hat{P} = 3$ replicas of a truncated raised-cosine pulse each delayed by $\hat{\tau}_{p,n}$ and weighted by $\hat{J}_{p,n} = \hat{\varepsilon}_{p,n}\hat{G}_{p,n}$, respectively, followed by chip-rate sampling.

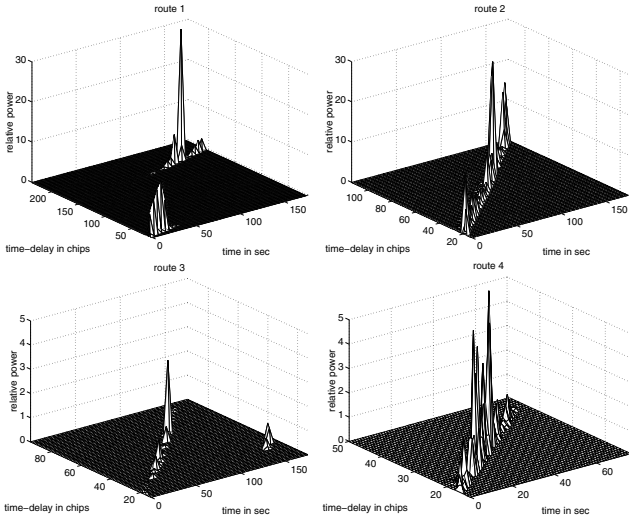

Fig. 2. Power vs. IR coefficient and time of the channel recordings collected along four different routes in Laval, a suburban area of Montreal, at vehicular speed below 30 Km/h (note synchronization hops in routes 1 and 3 due to channel sounder imperfections).

matrix $\mathbf{H}_n$ by its parametric decomposition, under structural constraints, as the the product of an $M \times P$ spatial channel matrix $\mathbf{J}_n$ and a $P \times L$ temporal channel matrix $\mathbf{D}_n^T$. Indeed, $\mathbf{J}_n = \mathbf{G}_n\mathbf{\Upsilon}_n$ is itself the product of $\mathbf{G}_n = [G_{1,n}, \ldots, G_{P,n}]$, the $M \times P$ column-wise normalized spatial channel matrix, and $\mathbf{\Upsilon}_n = \text{diag}\,[\varepsilon_{1,n}, \ldots, \varepsilon_{P,n}]$, the $P \times P$ diagonal matrix of normalized power ratios over multipaths $\varepsilon_{p,n}^2$ (*i.e.*, $\sum_{p=1}^{P} \varepsilon_{p,n}^2 = 1$). More importantly, each column of $\mathbf{D}_n = [D_{1,n}, \ldots, D_{P,n}]$ belongs to a *temporal manifold*, *i.e.*, its vector elements are known functions of a given parameter, namely the corresponding time delay $\tau_{p,n}$ of the p-th multipath:

$$D_{p,n} = [\rho_c(-\tau_{p,n}), \rho_c(T_c - \tau_{p,n}), \ldots, \rho_c((L-1)T_c - \tau_p)]^T, \quad (2)$$

where $\rho_c(t)$ is a truncated raised-cosine pulse which corresponds to the correlation function of the square-root raised-cosine shaping-pulse $\phi(t)$.

B. Overview of STAR

The core idea of STAR is the following: A main channel estimation module, referred to as decision feedback identification (DFI) in [1], provides a coarse *unconstrained* estimate $\tilde{\mathbf{H}}_n$ of the spatio-temporal channel. In an analysis step, a space-time separation or decomposition of the channel follows by successive extraction of the temporal channel matrix $\hat{\mathbf{D}}_n$ (*i.e.*, synchronization) and the spatial channel matrix $\hat{\mathbf{J}}_n$. In a synthesis step, a space-time reconstruction of the channel then provides a far more accurate constrained estimate [1]:

$$\hat{\mathbf{H}}_n = \underbrace{\hat{\mathbf{J}}_n\hat{\mathbf{D}}_n^T = \hat{\mathbf{G}}_n\hat{\mathbf{\Upsilon}}_n\hat{\mathbf{D}}_n^T}_{\text{ST channel synthesis}}, \quad (3)$$

by structure fitting along the nominal decomposition of the channel in (1) and (2) of the PCM model. A final combining step exploits the *constrained* channel estimate $\hat{\mathbf{H}}_n$ to extract the signal component $\hat{s}_n$ using simple MRC [1] or interference suppression [2], [5]. For simplicity here, we explain the concept and advantages of the analysis/synthesis-based design of STAR following the illustrations in Fig. 1.

The power of the spatio-temporal channel $\mathbf{H}_n = [H_{n,1}, \ldots, H_{n,k}, \ldots, H_{n,L}]$ is depicted in Fig. 1-a. It suggests that seven coefficients $H_{n,k}$, at least, have non-negligible power. In Fig. 1-b, the power of the despread observation $\mathbf{Z}_n$ of Eq. (1) shows that these seven most desired channel components are buried in noise. Conventional correlator-type receivers would average unmodulated post-correlation observations over time to bring these useful channel coefficients above a detection threshold. In contrast, the DFI module in STAR identifies the channel blindly using simple adaptive subspace tracking [1]. As shown in Fig. 1-c, the resulting unconstrained estimate $\tilde{\mathbf{H}}_n = [\tilde{H}_{n,1}, \ldots, \tilde{H}_{n,k}, \ldots, \tilde{H}_{n,L}]$ constantly keeps the power of most of the desired channel components above the rest of the coefficients (which may sporadically exceed the detection threshold unnoticed [1]). Yet, it offers only a coarse estimate of the actual channel coefficients in Fig. 1-a.

It is at this stage that the analysis/synthesis design features contribute significantly to the enhanced performance of STAR. Exploiting the parametric decomposition of the channel in Eqs. (1) and (2), STAR extracts by a high-resolution technique the multipath time delays $\hat{\tau}_{p,n}$ and

		rte 1	rte 2	rte 3	rte 4
$\widehat{d\tau/dt}$ [ppm]		0.10	0.14	0.12	0.10
$\frac{\bar{\varepsilon}_p^2}{\bar{\varepsilon}_1^2}$ [dB]	1^{st} path	0	0	0	0
	2^{nd} path	-3.9	-4.3	-3.8	-4.3
	3^{rd} path	-7.8	-8.0	-7.7	-7.7
$\overline{\Delta f}$ [Hz]		179	61	89	120
$\hat{f}_D$ [Hz]		42	30	41	10
$\hat{v}_{\max}$ [Km/h]		23	17	22	6

Table I. Extracted channel parameters from data (delay drift $\widehat{d\tau/dt}$, average multipath power profile $\bar{\varepsilon}_p^2/\bar{\varepsilon}_1^2$, carrier frequency offset $\overline{\Delta f}$, maximum Doppler spread $\hat{f}_D$ or speed $\hat{v}_{\max}$).

their number $\hat{P}$ from the unconstrained channel estimate $\tilde{\mathbf{H}}_n$ depicted in Fig. 1-c. In Fig. 1-d, the multipath time delays are accurately located with a resolution unlimited by the sampling rate or the clock precision. Estimation of the normalized multipath amplitudes $\hat{\varepsilon}_{p,n}$ and the complex fading components $\hat{G}_{p,n}$ completes the analysis step and allows for reconstruction of the constrained channel estimate $\hat{\mathbf{H}}_n = [\hat{H}_{n,1}, \ldots, \hat{H}_{n,k}, \ldots, \hat{H}_{n,L}]$ in the synthesis step. In Fig. 1-e, the resulting enhanced channel estimate is the best constrained fit that can be extracted from the unconstrained estimate $\tilde{\mathbf{H}}_n$ depicted in Fig. 1-c.

III. Channel Parameters Estimation and Receiver Design Verification Results

A database of real-world radio-channel measurements was recently made available for this study by Microcell Solutions Inc (a Canadian wireless operator). The database contains, in a raw format, impulse response (IR) measurements of 5 MHz radio-channels recorded between a rooftop transmit antenna and a single receive antenna (*i.e.*, $M = 1$) mounted inside a mobile mini-van [6]. From this database, we have been able to exploit four IR recordings (see Fig. 2) conducted at the so-called site 132 in Laval (a suburban area of Montreal) [6]. They correspond to four different routes of the mini-van close to a mall in the suburban Laval area (*i.e.*, site 132).

Results of the channel parameters estimation from real-world measurements using the STAR receiver are summarized in Tab. III and explained in more details in the following sections.

A. Extraction of the Multipath Time Delays

We extract the multipath time delays from the channel measurements using STAR to verify its analysis/synthesis-based design and to illustrate both its time synchronization capability and its ability to generate realistic time evolution models for the multipath delays. In Fig. 3, we plot both the power contour of the four IR recordings as well as the corresponding multipath time delays extracted by STAR. In all four recordings, we find that the channel is characterized by a maximum number of three multipaths. Additionally, the time delays extracted for routes 1 and 3 further demonstrate the very fast tracking capabilities

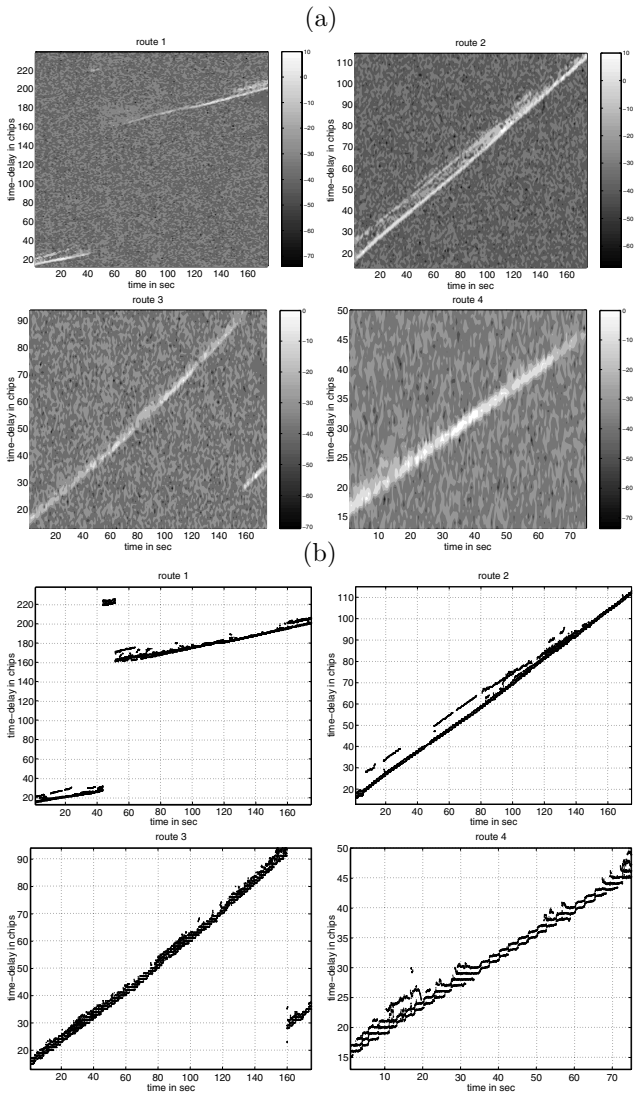

Fig. 3. Extraction of time delays illustrated: (a) power contour of the four IR recordings in Fig. 2, (b) corresponding multipath time delays extracted.

of STAR by instantly responding to very large time delay hops.

Besides allowing timely extraction of the channel parameters, analysis/synthesis-based STAR enables online dynamic modeling of their time evolution from real-world realizations. The time delay profiles extracted in Fig. 3-b are only examples that clearly illustrate its much broader dynamic characterization capability. They particularly suggest for the four channel recordings considered that time delays could evolve linearly in time in the long term, with a delay-drift or slope $\widehat{d\tau}$ specifically ranging here between 0.10 and 0.14 ppm (particle per million). A closer look to the time variations suggest slightly different drifts between paths for route 2 and shorter-term sinusoidal oscillations around the linear drift for route 4.

B. Extraction of the Multipath Components

Time-variations of multipath amplitudes may have an impact on the acquisition and tracking capabilities of a

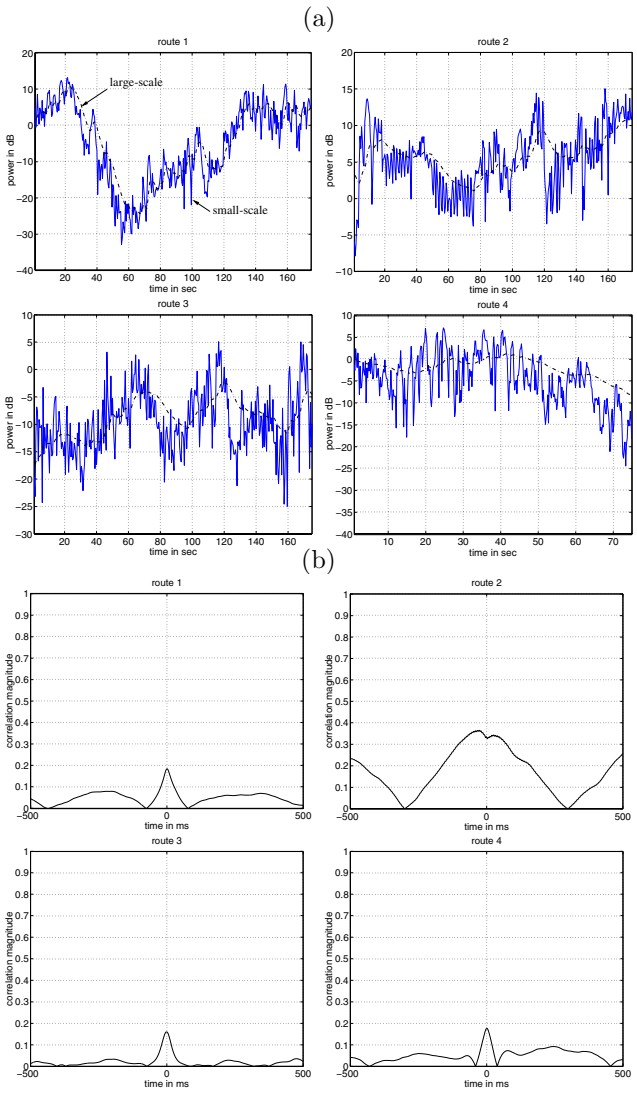

Fig. 4. Extraction of multipath components illustrated: (a) power profile of the 1st multipath fading component, (b) magnitude of correlation factor between envelopes of 1st and 2nd multipath components.

synchronization module and consequently on the performance of enhanced CDMA array-receivers. In Fig. 4-a we plot the dynamic power profile of the first multipath component as extracted by STAR. The other components, omitted for lack of space, show the same large-scale fading variations. These can be approximated by long-term averaging or smoothing as illustrated in dashed line in Fig. 4-a. However, the three paths have quasi-uncorrelated small-scale fading variations, as illustrated in Fig. 4-b between the 1st and 2nd multipaths. Indeed, the correlation factor does not exceed 0.2 for all but the second route, where it is a little higher at around 0.35. This result is very significant in that it strongly suggests that the analysis/synthesis-based receiver STAR is able to decompose the channel into few quasi-independent components using real-world data.

From the dynamic power profiles of the multipath components, STAR is also able to extract the corresponding average multipath power profile $\frac{\bar{\varepsilon}_p^2}{\bar{\varepsilon}_1^2}$ by simply taking $\bar{\varepsilon}_p^2$ as the mean over time of the normalized multipath power fraction estimate $\hat{\varepsilon}_{p,n}^2$. As suggested in Tab. III, the typical multipath power profile found for the suburban measurement environment is (0, -4, -8) dB.

C. Extraction of the Carrier Frequency Offset

We verify the analysis/synthesis-based design of STAR over real-world data by illustrating its ability to generate realistic time evolution models for the CFO (currently unavailable to our knowledge).

In Fig. 5-a, we plot as a reference the contour of the power spectral density (PSD) of the 1st multipath component extracted in Fig. 4-a without CFOR. In Fig. 5-b, we plot the dynamic CFO profile extracted by STAR directly from the IR measurements. These figures clearly indicate that the CFOR module of STAR is able to track instantly and accurately the shifts of the Doppler spectrum from 0 due to CFO. This remarkable performance is better illustrated in Fig. 5-a where the average CFO $\bar{\Delta}f$ (from Fig. 5-b) perfectly matches with the shift from 0 of the average PSD (from Fig. 5-c). It confirms the capacity of STAR to eliminate the CFO and the resulting SNR losses from real-world measurements and opens out onto the possibility of modeling the CFO realizations. Furthermore, it enables estimation of the maximum Doppler spread (or speed) in the presence of CFOs as discussed in the next subsection.

D. Extraction of the Maximum Doppler Spread

Mobility degrades the performance of synchronization both in time and frequency. It also degrades channel identification and tracking. Below, we exploit the CFOR capabilities of STAR shown earlier to propose a simple technique for speed estimation in the presence of CFO and illustrate its performance using real-world measurements.

Previous Doppler estimators [7], [8] assume a U-shaped Jakes' spectrum centered on zero. Here, we modify the nominal spectrum, first, by centering it around the CFO estimate $\hat{\Delta}f$, and second, by replacing its U shape by a flat one. Indeed, the PSDs extracted from the measurements in Fig. 4-a did not have a Jake's spectrum (see average PSD in Fig. 5-c). Actually, the U-shaped Jakes' spectrum reflects only a particular 2D geometry of scatterers. In the absence of any *a priori* information on the scatterers' positions, we assume a 3-D isotropically scattered field that results in a uniform spectrum [9]. With the above modifications, the ML-based Doppler estimator proposed in [7] reduces to a very simple procedure that automatically measures the mainlobe width $2\hat{f}_D$ of the PSD around the CFO estimate $\hat{\Delta}f$ [4]. Using each PSD in Fig. 5-a, however, this technique can also provide continuous (or more frequent) estimation of the maximum Doppler as shown in dashed line in Fig. 5-b. The resulting speed estimates are given in Fig. 5-d.

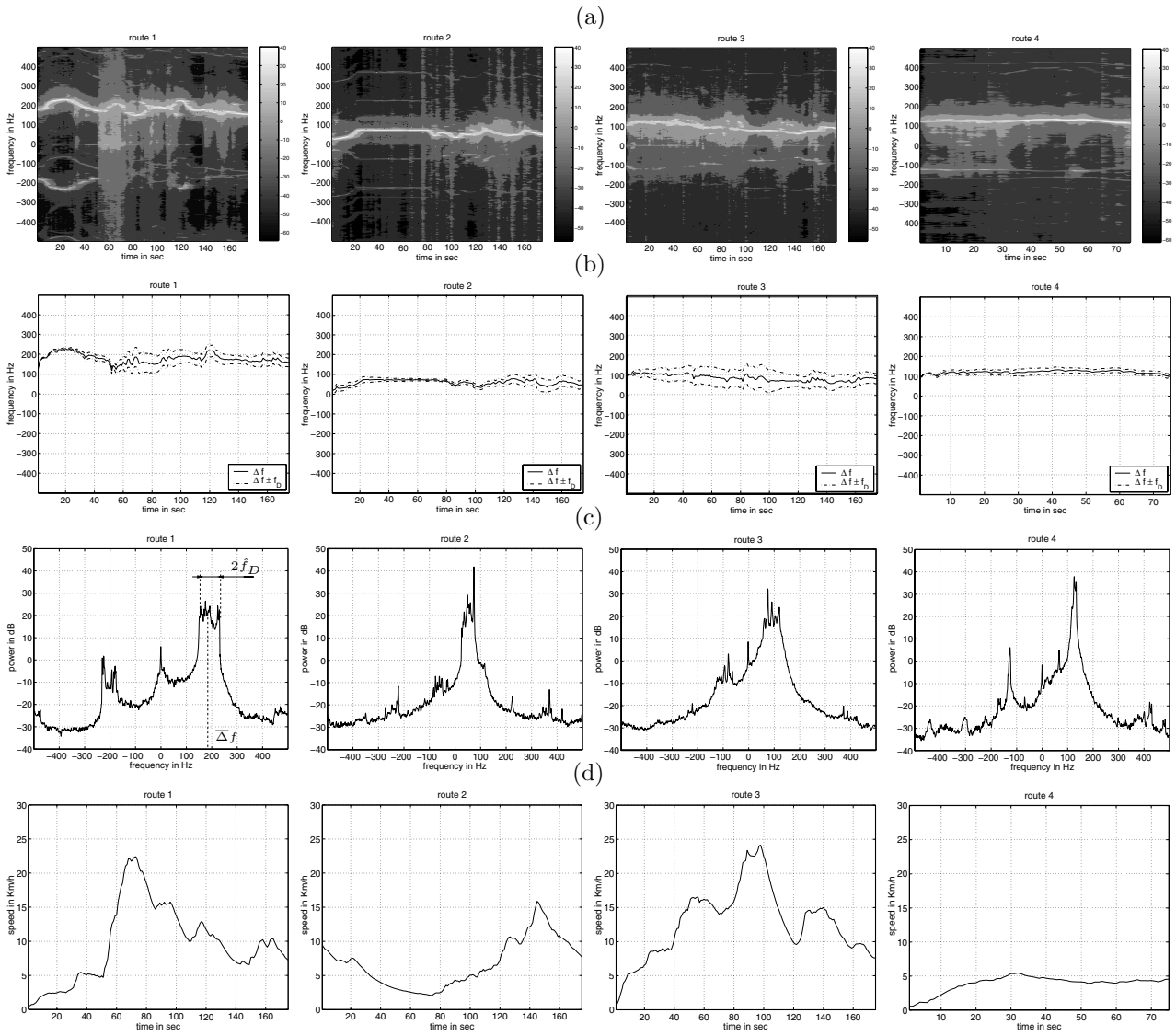

Fig. 5. Extraction of the carrier frequency offset illustrated: (a) power spectral density contour of the 1st multipath component, (b) extracted carrier frequency offset (maximum Doppler spread around CFO is in dashed line), (c) average PSD of the 1st multipath component, (d) estimated speed.

IV. Conclusions

In this work, we verified the analysis/synthesis-based design of STAR by illustrating its ability of instantly extracting the channel parameters (time delays and drifts, multipath components and average multipath power profiles, CFOs, Doppler spread or speed) from measured data and its ability of monitoring and adapting online to their time evolution in real-world propagation conditions.

References

[1] K. Cheikhrouhou, S. Affes, and P. Mermelstein, "Impact of synchronization on performance of enhanced array-receivers in wideband CDMA networks," *IEEE JSAC*, vol. 19, no. 12, pp. 2462–2476, Dec. 2001.

[2] H. Hansen, S. Affes, and P. Mermelstein, "High capacity downlink transmission with MIMO interference subspace rejection in multicellular CDMA networks," *EURASIP JASP*, vol. 2004, no. 5, pp. 707–726, May 2004.

[3] B. Smida, S. Affes, and P. Mermelstein, "Joint time-delay and frequency offest synchronization for CDMA array-receivers," in *Proc. of IEEE SPAWC'03*, Rome, Italy, Jun. 2003, pp. 499–504.

[4] K. Cheikhrouhou, S. Affes, A. Elderini, B. Smida, P. Mermelstein, B. Sultana, and V. Sampath, "Design verification and performance evaluation of an enhanced wideband CDMA receiver using channel measurements," *EURASIP JASP*, to appear, 3rd Quarter 2005, in press.

[5] S. Affes, K. Cheikhrouhou, and P. Mermelstein, "Enhanced interference suppression for spectrum-efficient high data-rate transmissions over wideband CDMA networks," in *Proc. of IEEE ICASSP'03*, vol. IV, Hong Kong, April 2003, pp. 469–472.

[6] S. Aridhi *et al.*, "Third generation trial, final report - phase 1," Microcell Connexions, Montreal, Tech. Rep., Mar. 1999.

[7] H. Hansen, S. Affes, and P. Mermelstein, "A Rayleigh Doppler frequency estimator derived from ML theory," in *Proc. of IEEE SPAWC'99*, Annapolis, USA, May 1999, pp. 382–386.

[8] M. Ghogho, A. Swami, and T. Durrani, "Blind synchronization and Doppler spread estimation of MSK signals in the context of time-selective fading channels," in *IEEE ICASSP'2000*, vol. 5, Jun. 2000, pp. 2665–2668.

[9] R. H. Clarke and W. L. Khoo, "3-D mobile radio channel statistics," *IEEE Trans. on VT*, vol. 46, no. 3, pp. 798–799, Aug. 1997.